ELSEVIER

Applied Surface Science 181 (2001) 35–50

applied surface science

www.elsevier.com/locate/apsusc

Study of mechanism of electroless copper coating of fly-ash cenosphere particles

S. Shukla[a], S. Seal[a,*], J. Akesson[a], R. Oder[b], R. Carter[c], Z. Rahman[a]

[a]*Advanced Materials Processing and Analysis Center (AMPAC) and Mechanical, Materials and Aerospace Engineering (MMAE) Department, University of Central Florida, Orlando, FL 32816, USA*

[b]*Energy Strategy Assoc., Inc., P.O. Box 2494, Palm Beach, FL 33480-2494, USA*

[c]*US Natural Sources, Inc., P.O. Box 256, Belle Vernon, PA 15012, USA*

Received 16 March 2001; accepted 29 April 2001

Abstract

Electroless Cu coating process involving Sn–Pd catalyst system is successfully utilized to coat Cu on the surface of fly-ash cenosphere particles to impart electrical conductivity to these non-conducting oxide ceramic particles. The low density Cu-coated cenosphere particles may be utilized for manufacturing conducting polymers for EMI shielding applications. This is the first report in the open literature to investigate the electroless Cu coating of fly-ash cenosphere particles in detail. Extensive characterization of coated particles is carried out by scanning electron microscopy (SEM)/energy dispersive spectroscopy (EDX), X-ray photoelectron spectroscopy (XPS), focused ion beam spectroscopy (FIB), and X-ray diffraction (XRD) techniques to study the coating process and to show successful deposition of pure Cu. The mechanism of electroless Cu coating is mainly studied with the help of XPS, which shows the reduction of $PdCl_2$ (activator) catalyst on the surface of cenosphere particles by $SnCl_2$ (sensitizer) to produce pure Pd^0 clusters, which subsequently act as nucleation sites for Cu deposition. The concept of XPS core-level binding energy (BE) shift due to small cluster size is utilized to predict the size of pure Pd^0 clusters deposited on the fly-ash particle surface after the activation step. For the first time, the use of FIB technique is described and demonstrated to determine directly the Cu coating thickness.

PACS: 81.15.Pq

Keywords: Cenosphere; Electroless coating; Copper; XPS; SEM; FIB

1. Introduction

Fly-ash cenospheres are generated in large amounts as a by-product in thermal power plant and pose major disposal problems. Research is in progress to find out the various ways to utilize this by-product to prevent any environmental problem as well as effectively use them to produce new usable materials. Fly-ash has a very low density (<0.7 g/cm^3) and can be used to produce lightweight metal matrix composites. They have crystal structure similar to that of soft ferrite and hence possess very low electrical conductivity. During the last decade, fly-ash cenosphere particles have been dispersed in different matrices, such as polyester resins [1], cement [2], and nickel [3] for producing

* Corresponding author. Tel.: +1-407-823-5277; fax: +1-407-823-0208.
E-mail addresses: svs73464@pegasus.cc.ucf.edu (S. Shukla), sseal@pegasus.cc.ucf.edu (S. Seal).

0169-4332/01/$ – see front matter
PII: S0169-4332(01)00341-5

composite materials in the bulk and coating forms for variety of industrial applications. Fly-ash is a non-conducting ceramic material, however the desired conductivity may be imparted to these particles by depositing Cu on their surface. Due to their low density, these Cu-coated fly-ash cenospheres may find applications as a conducting filler in polymer matrices to produce conducting polymers as well as in a lead matrix to produce lead base composite material used in automobile industries. However, the use of Cu-coated cenosphere particles for these applications have not yet been reported in the open literature. Moreover, there is also no report at present related to the electroless Cu coating of fly-ash cenosphere particles.

Electroless method of Cu coating is a versatile process to coat pure metallic copper on the ceramic surfaces without consuming any external electric power. Successful Cu coating of particles such as mica [4], graphite [5], and iron [6] particles by electroless method have been reported earlier in the literature. In the present investigation, we demonstrate for the first time the electroless Cu coating of fly-ash cenosphere particles. We also investigate in detail the mechanism of electroless Cu coating of fly-ash cenosphere particles with the help of X-ray photoelectron spectroscopy (XPS) along with other analytical techniques such as scanning electron microscopy (SEM), energy dispersive spectroscopy (EDX), X-ray diffraction (XRD) and focused ion beam spectroscopy (FIB). The use of powerful technique such as FIB to measure directly the Cu coating thickness is demonstrated for the first time in this investigation.

2. Experimental

2.1. Materials

Fly-ash cenosphere particles having a low density of $<0.7\ g/cm^3$ used in the present investigation were supplied in two different batches by Coal Resources Inc., USA. Fly-ash cenosphere particles from both batches were used for the electroless Cu coating experiments. The choice of the batch for the coating experiments was however as per convenience and is mentioned whenever required.

2.2. Chemicals

The chemicals used for electroless Cu coating of fly-ash cenosphere particles included $SnCl_2$ (anhydrous min. 99%), NaOH (99.3%), $NaKC_4H_4O_6$ (min. 99%), HCHO (37 wt.%) (from Sigma, USA), HCl (37 wt.%) and $PdCl_2$ (99.9%, metals basis, Pd 59.78%) (from Aldrich, USA).

2.3. Electroless Cu coating of fly-ash cenosphere particles

The general sequential steps involved in the present electroless Cu coating process were as follows. The as-received fly-ash cenosphere particles were first stirred in the acidic $SnCl_2$ bath, containing 5 g/l of $SnCl_2$ and 30 ml/l of conc. HCl acid, for 1 h (sensitization step). The sensitized particles were filtered off, then transferred to acidic $PdCl_2$ bath containing $PdCl_2$ (0.4–1.0 g/l) and conc. HCl acid (5 ml/l) and stirred in this bath for 50 min (activation step). The activated particles were filtered off and washed thoroughly in de-ionized water. The particles were then transferred to the coating bath involving 5 g/l NaOH, 30 g/l $NaKC_4H_4O_6$, 12 g/l $CuSO_4$, and 20 ml/l HCHO, for actual Cu-deposition. The Cu-coated particles were then dried in a vacuum oven at 110°C for 1 h. Fly-ash cenosphere particles used in the present investigation provided non-catalytic surface for Cu coating process. Hence, electroless Cu coating of such surface requires a two-step process, involving sensitization and activation, to make them suitable for subsequent Cu deposition. To achieve this, acidic $SnCl_2$ solution was used as sensitizer whereas acidic $PdCl_2$ solution was used as an activator. Under these conditions, following reaction occurs on the cenosphere particle surface during the activation step,

$$Sn^{2+} + Pd^{2+} \rightarrow Sn^{4+} + Pd^0 \quad (1)$$

In this reaction, Sn^{2+} can reduce Pd^{2+} ions since standard oxidation–reduction potential of Sn^{4+}/Sn^{2+} couple (0.15 V) is less than that of Pd^{2+}/Pd^0 couple (0.987 V) [7]. Under the catalytic action of Pd^0, Cu cations get deposited onto the surface by capturing electrons furnished by a common reducing agent (HCHO) via following chemical reactions,

$$HCHO + OH^- \rightarrow H_2 + HCOO^- \quad (2)$$

$$Cu^{2+} + 2HCOO^- + 3H_2 \rightarrow Cu + 2HCHO + 2H_2O \quad (3)$$

The overall reaction can be written as

$$Cu^{2+} + H_2 + 2OH^- \rightarrow Cu + 2H_2O \quad (4)$$

The deposited Cu atoms then act as a self-catalyst for further Cu deposition and well-developed Cu coating on the fly-ash cenosphere particle surface is then obtained via this electroless coating process.

2.4. Characterization of uncoated and Cu-coated fly-ash cenosphere particles

A modified JEOL-SEM 4600 was used to analyze the cenosphere particle size distribution in two different batches of fly-ash cenosphere particles while EDX analysis was performed to understand the chemistry of uncoated and Cu-coated particles. The structure analysis of Cu-coated fly-ash cenosphere surface is carried out by using Rigaku XRD Technique utilizing Cu Kα X-radiation of wavelength 1.54 Å to confirm the deposition of pure Cu on the fly-ash cenosphere particle surface. The variation in the surface chemistry of fly-ash cenosphere particles during the electroless Cu coating process was studied with the help of 5400 PHI ESCA (XPS) spectrometer having a base pressure of 10^{-10} Torr using Al Kα X-radiation (1486 eV, linewidth 0.7 eV) at a power of 350 W. Small amount of particles were removed after each step involved in the electroless coating process for XPS analysis to understand the mechanism of electroless Cu coating of fly-ash cenosphere particles. Both survey and high-resolution narrow spectra were recorded with electron pass energy of 44.75 and 35.75 eV, respectively, to achieve the maximum spectral resolution. Narrow and high resolution scans were conducted for key elements (Sn, Pd, Cl, Cu and C) to understand the variation in the oxidation states of these elements during the coating process. The binding energy (BE) of the Au $4f_{7/2}$ at 84.0 ± 0.1 eV was used to calibrate the BE scale of the spectrometer. Any charging shifts produced by the samples were carefully removed by using a BE scale referred to C 1s BE of the hydrocarbon part of the adventitious carbon line at 284.6 eV [8]. A method described by Sherwood was adopted to remove non-linear backgrounds from the spectra [9]. Non-linear least square curve fitting was performed using a Gaussian/Lorentzian peak shape after the background removal [9,10].

FIB analysis was performed on the Cu-coated particles for directly measuring the Cu coating thickness under different processing conditions. A Fei FIB200, with 7 mm probe size and a 30 kV liquid metal ion source, was used in the present investigation for this purpose. The thickness measurement via FIB was accomplished by milling a hole through one of the Cu-coated cenosphere particle surface and then tilting the sample stage to see the cross-section of the milled hole. In order to protect the Cu coating from getting destroyed while milling the hole, solid platinum (Pt) was deposited as a thin strip on the Cu-coated cenosphere particle surface before milling the hole. A hole was then milled by ion sputtering (20,000 pA ion current) through the Cu coating down into the hollow cenosphere particle interior. A finer cut was then made with 10 pA ion current next to the Pt strip. A lower current was used for the fine cut to avoid re-deposition on the cross-section of the milled hole. The milling invariably milled away half of the platinum strip. The particle with a surface milled hole was then tilted by 45° and the thickness of the coating was measured, which was further corrected for obtaining true thickness by multiplying the measured thickness by a factor of $\sqrt{2}$. The Cu–Pt interface was used as the reference line for the thickness measurement.

3. Results and discussion

3.1. SEM/EDX analysis

The chemical composition of both batches of cenosphere particles were same, however, they differed in the particle size distribution as indicated respectively by EDX and SEM analyses. The measured particle size distributions of the as-received cenosphere particles for the two batches are presented in Fig. 1. In the batch-I (Fig. 1(a)), the particle size distribution is very wide ranging from 70 to 280 μm with mean particle size of 115 μm. In the batch-II (Fig. 1(b)), the average particle size is 70 μm with the overall size range of 30–92 μm. Thus, fly-ash cenosphere particles in the batch-II are finer and for given amount of powder provide more surface area than that provided by the particles in the batch-I. These fly-ash cenosphere

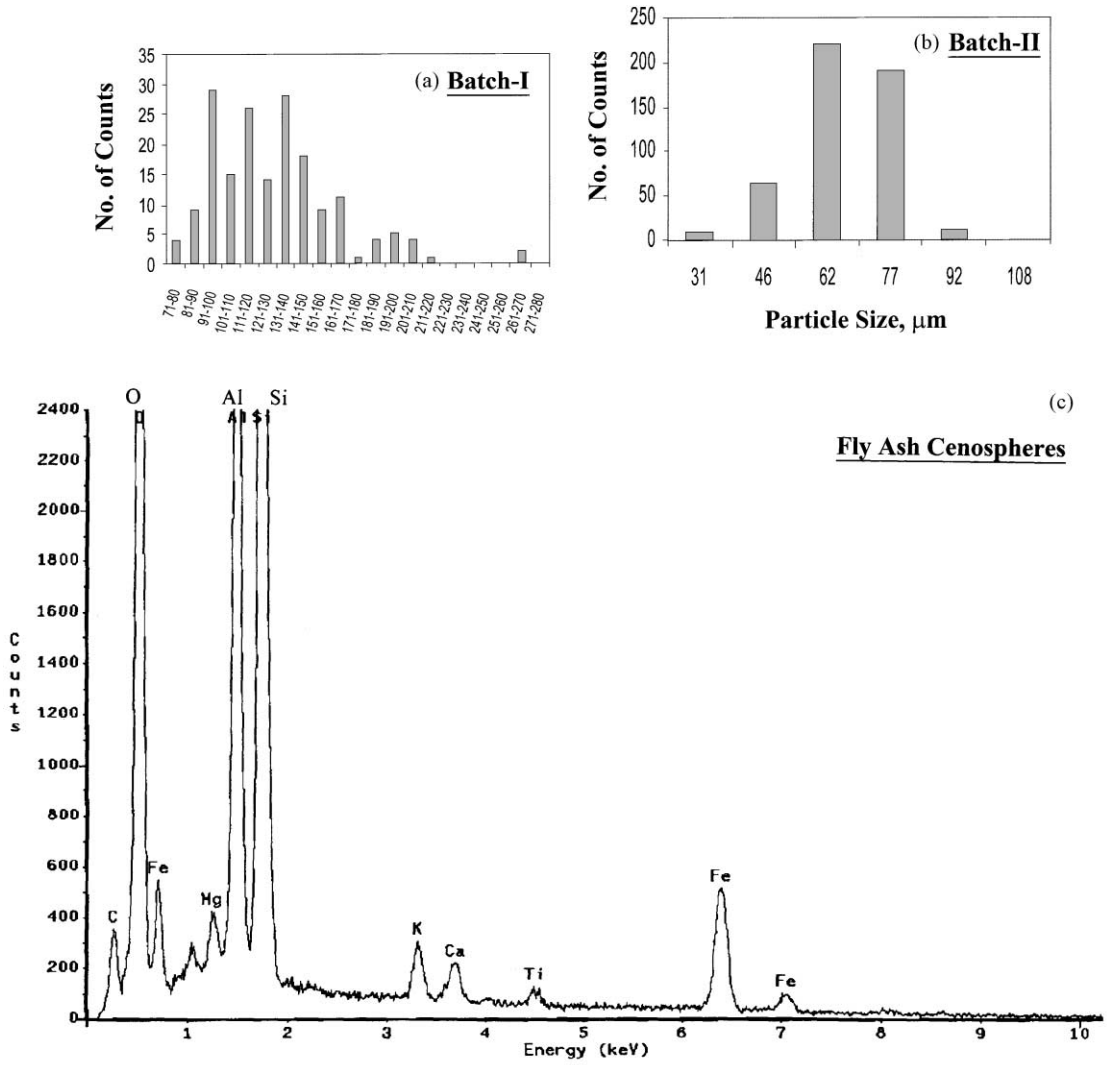

Fig. 1. (a and b) Particle size distribution obtained from SEM micrographs for two different batches of as-received fly-ash cenosphere particles and (c) EDX analysis of uncoated fly-ash cenosphere particles from batch-I showing the presence of Si, Al and Fe as major elements and K, Ca, Mg, Ti as minor elements. No Cu is detected for uncoated particles.

particles are mainly composed of mixture of oxides such as SiO_2, Al_2O_3, and Fe_2O_3 as indicated by the EDX analysis (Fig. 1(c)), for batch-I cenosphere particles. Various trace elements, such as K, Ca, Mg, Ti and C are also present.

SEM micrographs of uncoated and Cu-coated fly-ash cenosphere particles from batch-I are presented in Fig. 2. The as-received cenosphere particles have spherical surface morphology as indicated by Fig. 2(a). In Fig. 2(b), all the particles are observed to be uniformly coated by the present electroless coating method. It is also to be noted that even the Cu-coated particles exhibit spherical surface morphology indicating the uniform nature of the Cu coating obtained by this technique. SEM micrographs of one typical uncoated and Cu-coated fly-ash cenosphere particles are respectively presented in Fig. 2(c) and (d). The uniform coating is also evident at high magnification (Fig. 2(d)), where some clusters are also seen to be deposited on the surface. EDX analysis

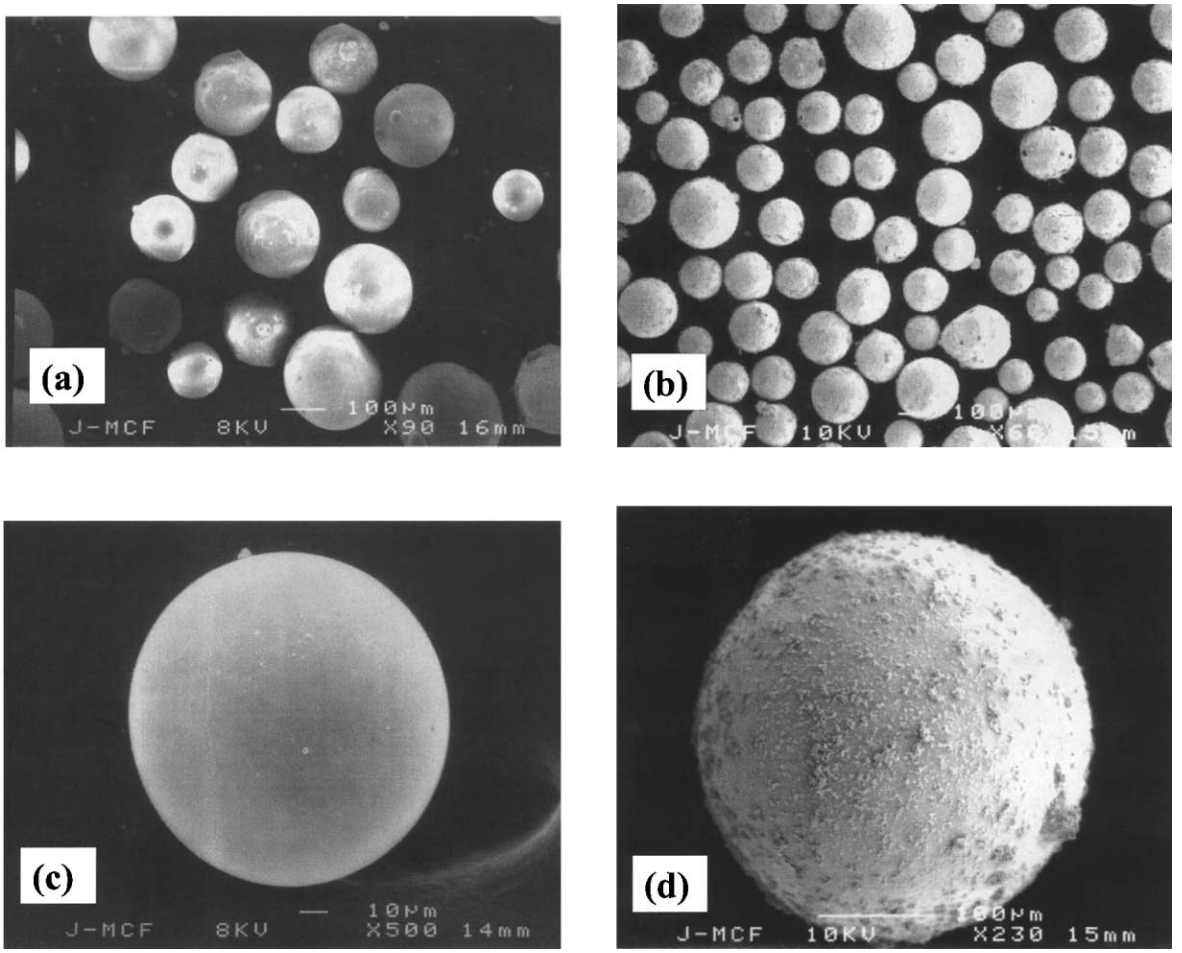

Fig. 2. SEM micrographs of uncoated cenosphere particles from batch-I at (a) low and (c) high magnifications, and Cu-coated cenosphere particles at (b) low and (d) high magnifications.

of Cu-coated cenosphere particle surface (Fig. 3(a)), shows the prominence presence of Cu along with the other underlying substrate elements such as Si, Fe, Al and K. It is to be noted that the peak corresponding to Cu was not present in Fig. 1(c) and it appears only after electroless coating process, indicating successful Cu deposition on the cenosphere particle surface by the present electroless technique. At very high magnification (Fig. 3(b)), the Cu-coated surface reveals the presence of nanoparticles of size 200–300 nm. EDX analysis of these nanoparticles showed that these particles are primarily Cu. It appears that during the electroless Cu deposition, uniform Cu coating over the sensitized and activated cenosphere particle surface develops through Cu nanoparticles formation. Thus, SEM and EDX analysis suggest the successful Cu deposition on the surface of fly-ash cenosphere particles by the present electroless process. However, confirmation of the oxidation state of the deposited Cu needed XPS analysis.

3.2. XPS analysis

Fig. 4 represents the broad scan XPS survey spectra for cenosphere particles undergoing different processing conditions. After the sensitization in the acidic $SnCl_2$ bath (Fig. 4(a)), the cenosphere particle surface shows the presence of Sn and Cl. After the activation

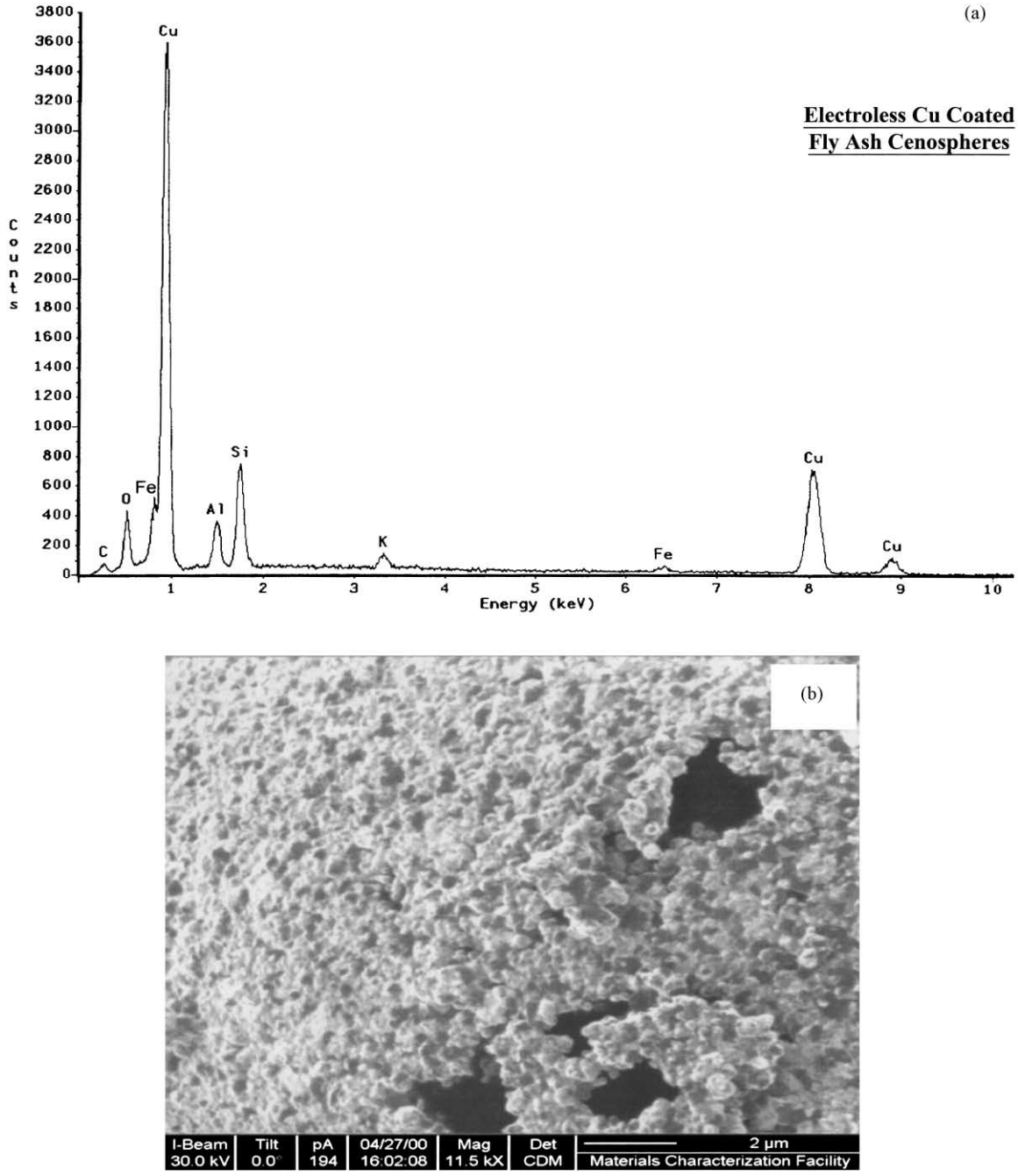

Fig. 3. (a) EDX analysis of Cu-coated fly-ash cenosphere particles showing the presence of Cu as a major element on the particle surface indicating successful Cu coating of fly-ash cenosphere particles. (b) Cu-coated fly-ash cenosphere particle surface at high magnification showing the presence of Cu nanoparticles of size 200–300 nm. The photograph was obtained during FIB analysis of the Cu coating thickness measurement.

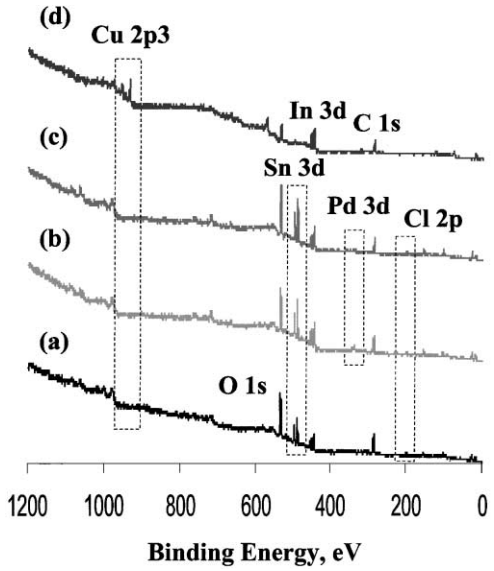

Fig. 4. XPS survey spectra for Cu-coated cenosphere particles — (a) sensitized, (b) activated, (c) washed and (d) Cu-coated samples. The particles were pressed against indium (In) foil for the analysis.

in the acidic $PdCl_2$ bath (Fig. 4(b)) additional presence of Pd is detected on the surface of cenosphere particle. Even after thorough washing of the activated particles in de-ionized water, no further change is observed in the survey spectrum (Fig. 4(c)). However, after the final coating step in the electroless coating bath (Fig. 4(d)), only Cu is detected on the cenosphere particle surface, which indicates thick Cu coating developed on the cenosphere particle surface. For XPS analysis, the cenosphere particles were pressed against In foil and hence peaks corresponding to In were also recorded along with those of other elements during the broad scan analysis. However, this peak is of no significance in this investigation.

The BE and FWHM values obtained via high resolution narrow scan XPS analysis for core-levels of major elements such as Sn, Pd, Cl and Cu, observed on the cenosphere particle surface during the coating process, are tabulated, respectively, in Tables 1 and 2. The BE values are compared with the literature values for proper compound identification. The BE and FWHM values obtained for powder chemicals ($SnCl_2$, $PdCl_2$ and $CuSO_4$ powders), used in the present electroless coating experiments, were also recorded and are, respectively, tabulated in Tables 1 and 2 for reference.

Narrow and high resolution XPS scans for Sn $3d_{5/2}$, within the BE range of 475–500 eV, and Pd $3d_{5/2}$, within the BE interval of 325–355 eV were conducted, which revealed interesting changes in the spectral

Table 1
XPS core-level BE (±0.1 eV) values obtained for the major elements (Sn, Pd, Cl, and Cu) involved in the electroless Cu coating of fly-ash cenosphere particles[a]

	Binding energy (eV)			
	Pd $3d_{5/2}$	Sn $3d_{5/2}$	Cl $2p_{3/2}$	Cu $2p_{3/2}$
$PdCl_2$ powder	335.0 (Pd)	–	198.4 ($PdCl_2$)	–
	337.2 ($PdCl_2$)	–	198.4 ($PdCl_2$)	–
$SnCl_2$ powder	–	487.0 ($SnCl_2$)	198.7 ($SnCl_2$)	–
$CuSO_4$ powder	–	–	–	936.3 ($CuSO_4$)
Sensitized	–	486.9 ($SnCl_2$)	198.4 ($SnCl_2$)	–
Activated	335.9 (Pd)	487.1 ($SnCl_4$)	198.4 ($PdCl_2$)	–
	337.1 ($PdCl_2$)	487.1 ($SnCl_4$)	199.5 ($SnCl_4$)	–
Activated and washed	335.2 (Pd)	486.7 ($Sn(OH)_2$)	198.1 ($PdCl_2$)	–
	336.3 (PdO)	486.7 ($Sn(OH)_2$)	201.0 (?)	–
	337.6 ($PdCl_2$)	486.7 ($Sn(OH)_2$)	201.0 (?)	–
Cu-coated	–	–	–	931.6 (?)
	–	–	–	932.7 (Cu)
	–	–	–	933.8 (CuO)

[a] Respective values related to powder chemicals used are also tabulated for reference.

Table 2
FWHM (±0.1 eV) values obtained for the major elements (Sn, Pd, Cl, and Cu) involved in the electroless Cu coating of fly-ash cenosphere particles[a]

	FWHM (eV)			
	Pd $3d_{5/2}$	Sn $3d_{5/2}$	Cl $2p_{3/2}$	Cu $2p_{3/2}$
$PdCl_2$ powder	1.4 (Pd)	–	1.6 ($PdCl_2$)	–
	1.5 ($PdCl_2$)	–	1.6 ($PdCl_2$)	–
$SnCl_2$ powder	–	1.9 ($SnCl_2$)	1.8 ($SnCl_2$)	–
$CuSO_4$ powder	–	–	–	3.6 ($CuSO_4$)
Sensitized	–	1.8 ($SnCl_2$)	1.8 ($SnCl_2$)	–
Activated	1.9 (Pd)	1.9 ($SnCl_4$)	1.7 ($PdCl_2$)	–
	2.3 ($PdCl_2$)	1.9 ($SnCl_4$)	1.4 ($SnCl_4$)	–
Activated and washed	1.5 (Pd)	1.9 ($Sn(OH)_2$)	1.4 ($PdCl_2$)	–
	1.7 (PdO)	1.9 ($Sn(OH)_2$)	1.2 (?)	–
	1.7 ($PdCl_2$)	1.9 ($Sn(OH)_2$)	1.2 (?)	–
Cu-coated	–	–	–	1.5 (?)
	–	–	–	1.7 (Cu)
	–	–	–	2.3 (CuO)

[a] Respective values related to powder chemicals used in the process are also included.

features (see Figs. 5 and 6) occurring during different processing steps. In Fig. 5(a), Sn $3d_{5/2}$ BE level is observed at 486.9 eV while Cl $2p_{3/2}$ BE level (Table 1) is observed at 198.7 eV after sensitizing the cenosphere particles surfaces. Both of these BE values suggest the deposition of $SnCl_2$ on the cenosphere particle surface as these values match with those observed for $SnCl_2$ powder used in the sensitization step (Table 1).

After the activation of the sensitized particles in acidic $PdCl_2$ solution, the Sn $3d_{5/2}$ and Cl $2p_{3/2}$ BE level increase to 487.1 eV (Fig. 5(b)) and 199.5 eV (Table 1). This suggests increase in the oxidation state of Sn^{2+} probably to Sn^{4+} and the presence of Sn(IV) species, i.e. $SnCl_4$ on the cenosphere particle surface after the activation step, which is in accordance with the reaction (1). Moreover, after the activation step, Pd $3d_{5/2}$ BE level exhibits two components. The peak-I in Fig. 6(a) is observed at 335.9 eV (FWHM = 1.9 eV) and corresponds to Pd^0. The peak-II (Fig. 6(a)), is observed at 337.1 eV indicating the presence of $PdCl_2$ as it matches with that observed for $PdCl_2$ powder used in the activation step (Table 1). Thus, it appears that after the activation of the sensitized cenosphere particle surface in the acidic $PdCl_2$ solution, metallic

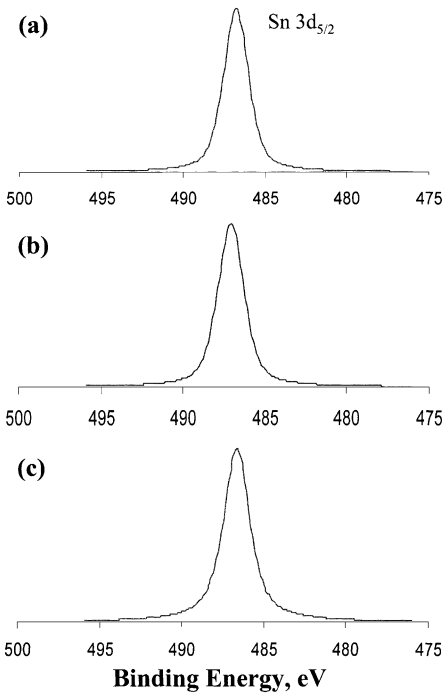

Fig. 5. XPS Sn $3d_{5/2}$ spectra for (a) sensitized, (b) activated and (c) washed particles. The peaks are identified as: (a) $SnCl_2$, (b) $SnCl_4$, and (c) $Sn(OH)_2$.

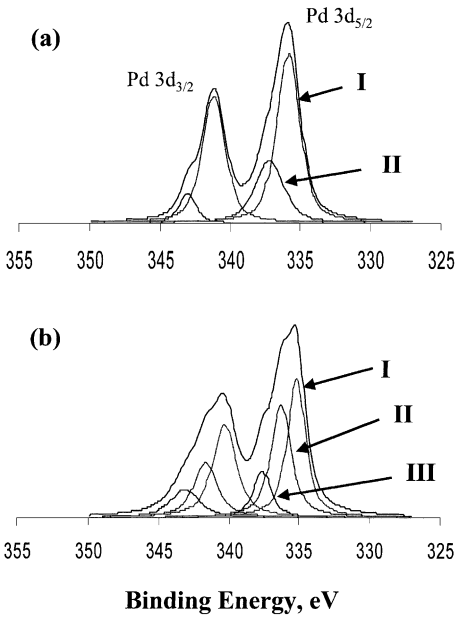

Fig. 6. XPS Pd $3d_{5/2}$ spectra for (a) activated and (b) washed particles. The peaks are identified as: in (a) I — Pd^0, II — $PdCl_2$ and in (b) I — Pd^0, II — PdO, III — $PdCl_2$.

Pd^0 clusters are deposited on the cenosphere particle surface, in accordance with the reaction (1), which further supports the increase in the oxidation state of Sn^{2+} to Sn^{4+} as mentioned earlier. Small amount of unreacted $PdCl_2$ is also observed on the activated surface. It is interesting to note that the BE level of 335.9 eV noted for Pd^0 clusters is shifted by +0.8 eV relative to the bulk value of pure metallic Pd (335.1 eV) reported in the literature [11,12]. Secondly, the FWHM of Pd $3d_{5/2}$ as obtained for Pd^0 clusters deposited on the cenosphere particle surface is also increased from 1.1 eV, related to the bulk Pd, to 1.9 eV (Table 2). Meenan et al. also observed a shift of +0.7 eV in Pd $3d_{5/2}$ spectrum during their investigation of electroless Cu deposition on $BaTiO_3$ ceramic substrate and attributed it to the Pd–Sn alloy formation [13]. In the present investigation, however, pure Sn peak is not detected in Fig. 5(b) after the activation step, and hence, the observed +ve BE shift in the Pd $3d_{5/2}$ spectrum cannot be explained on the basis of Pd–Sn alloy formation. Hence, we also eliminate the possibility of Pd–Sn alloy formation in the present investigation.

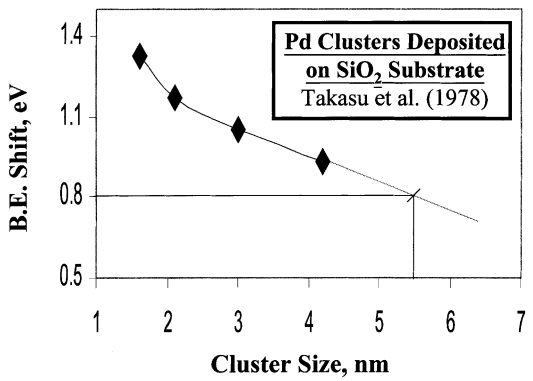

Fig. 7. Graph of core-level Pd $3d_{5/2}$ BE shift vs. Pd cluster size. The data is obtained from Takasu et al. [16]. The graph predicts Pd cluster size of ~5.5 nm for the BE shift of +0.8 eV.

On contrary, we ascribe the +ve shift of 0.8 eV observed in Pd $3d_{5/2}$ BE level to the Pd cluster size. The small size of Pd clusters may give rise to initial and final state effects during XPS analysis, which may be responsible for the +ve shift in the BE of core-level electrons in Pd clusters. In the literature, the initial state effect is related to the changes in the electronic structure with the change in cluster size while the final state effect is related to the +ve charge left on the surface of the cluster during the photoemission process [14,15]. Based on these two effects, increase in the BE and FWHM for the core-level peak with decrease in cluster size has been reported earlier for Pd clusters [16,17] and also for other transition metals (Au [18,19], Ag [19]). The present BE and FWHM

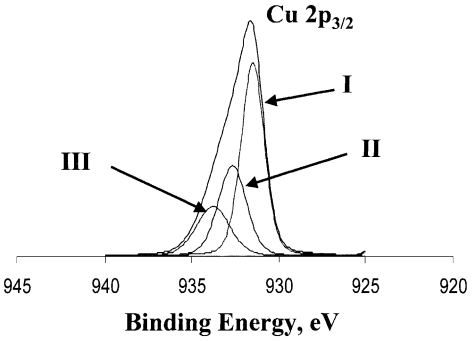

Fig. 8. XPS Cu $2p_{3/2}$ spectra for Cu-coated fly-ash cenosphere particles. The peaks are identified as: I — Cu complex, II — Cu(0) and III — CuO.

data obtained for Pd $3d_{5/2}$ peak, after the activation step (see Table 2) is observed to follow this trend. Hence, we believe here that +ve BE shift of 0.8 eV observed for Pd $3d_{5/2}$ BE level relative to bulk value is the effect of Pd cluster size and is not due to Pd–Sn alloy formation.

Since the earlier studies have shown that +ve BE shift is a function of cluster size [15–19] one can approximately predict the Pd cluster size deposited on the cenosphere particle surface from the +ve BE shift of 0.8 eV observed in the core-level Pd $3d_{5/2}$ spectrum related to Pd^0 clusters. Takasu et al. studied the changes in the core-level Pd $3d_{5/2}$ BE by depositing the Pd^0 clusters of different sizes on the amorphous silica substrate via vacuum deposition and observed that +ve shift in the Pd $3d_{5/2}$ BE level increases from 0.93 to 1.33 eV when the Pd^0 cluster size decreases from 4.2 to 1.6 nm [16]. Fig. 7, a graph of Pd $3d_{5/2}$ BE shift versus Pd^0 cluster size, is plotted by using the literature data to estimate the Pd cluster size (after the activation step) from the observed +ve shift in the Pd $3d_{5/2}$ BE level (Fig. 6(a)). The graph in Fig. 7 is

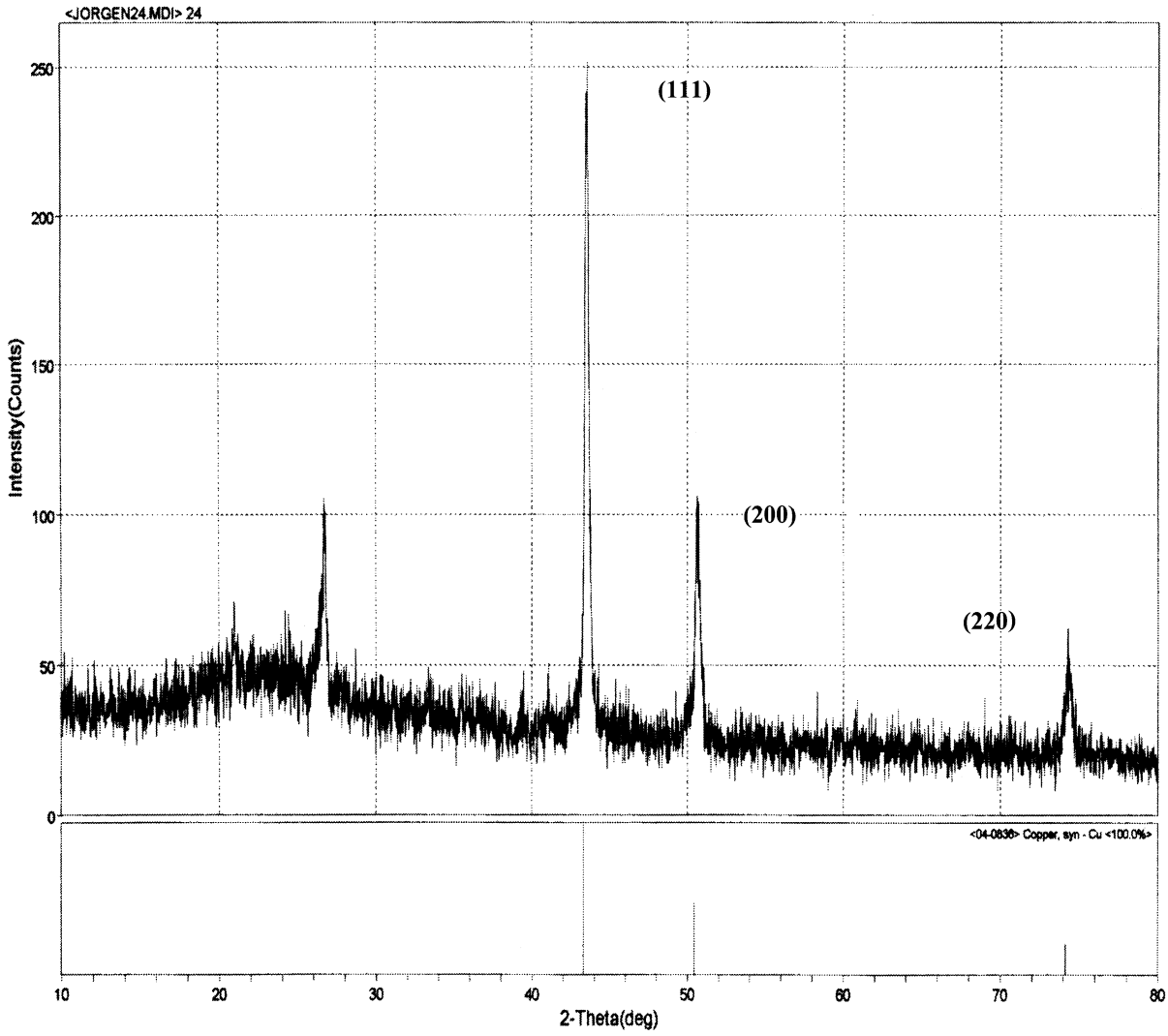

Fig. 9. XRD powder pattern obtained for Cu-coated fly-ash cenosphere particles. The peaks corresponding to bulk Cu, viz. (1 1 1), (2 0 0) and (2 2 0) are identified by comparison with the PDF-card (no. 04-0836) of JADE-SCAN software, shown in the lower part of the figure.

extrapolated beyond 4.2 nm cluster size for this purpose. We note that for the BE shift of +0.8 eV, the Pd^0 cluster size of 5.5 nm is predicted by the graph. Hence, we believe that after the activation of sensitized cenosphere particles in $PdCl_2$ solution, the Pd^0 clusters of ~5.5 nm average diameter have been deposited on the cenosphere particle surface, which act as nucleation sites for subsequent Cu deposition in the coating bath.

Thus, after the activation step, Pd^0 clusters of average diameter of 5.5 nm are detected on the cenosphere particle surface along with the presence of $PdCl_2$ (peak-II in Fig. 6(a)) and $SnCl_4$ species (Fig. 5(b)). In order to dissolve these species before actual Cu deposition, the activated cenosphere particles were washed thoroughly in de-ionized water. After de-ionized washing of the activated cenosphere particles, Sn $3d_{5/2}$ peak is observed to be shifted to lower BE side (486.7 eV) (Fig. 5(c)) and is attributed to the formation of $Sn(OH)_2$. Meenan et al. had reported similar formation $Sn(OH)_4$ from Sn(II) compounds during their investigation of electroless Cu deposition on $BaTiO_3$ ceramic substrate using Sn–Pd catalyst system [13]. As indicated in Fig. 6(b), after thorough washing in de-ionized water, in addition to Pd^0 peak, a peak at BE level of 336.3 eV is detected, which is not present before the washing step and it corresponds to PdO according to literature [20]. Moreover, even after thorough washing in de-ionized water, $PdCl_2$ is not eliminated completely from the surface of cenosphere particle. The presence of $Sn(OH)_2$ and $PdCl_2$ is detrimental to electroless Cu coating as they form a sheath, which may impair the catalytic activity of Pd^0 sites for subsequent Cu deposition [13].

The sensitized, activated and thoroughly washed particles are then immersed in the final coating bath for the actual Cu deposition. The XPS survey spectra of Cu-coated cenosphere particles (Fig. 4(d)), do not reveal the presence of Pd, Sn and Cl on the surface of Cu-coated cenosphere particle. Even by the EDX analysis (Fig. 3(a)), the presence of these elements could not be detected underneath the Cu coating. Since, well developed Cu coating is obtained after stirring the washed particles in the Cu coating bath, we believe that the sheathing of $Sn(OH)_2$ and $PdCl_2$ is dissolved completely by the electroless coating bath, exposing the catalytic Pd^0 sites, before the actual Cu deposition begins. Narrow XPS scan of Cu $2p_{3/2}$ within the BE interval of 920–945 eV, after the final Cu deposition, is shown in Fig. 8, where three peaks are identified. The peak-II is at 932.7 eV and corresponds to pure metallic Cu. The peak-III is at 933.8 eV and is related to CuO. These observations qualitatively suggest that pure Cu is successfully deposited on the cenosphere particle surface by the present electroless technique. However, some surface oxidation of deposited Cu has also occurred. Further, the peak-I is observed at 931.6 eV and is shifted to lower BE side relative to Cu(0) peak. The exact origin of this −ve shift is not yet known. However, it is to be noted that during the electroless Cu deposition, Cu may form an intermediate complex such as copper tartarate (CuT) before pure metallic Cu is deposited on the cenosphere particle surface. The peak-I may then be related to this type of intermediate complex Cu species, which might be present on the particle surface even after completion of the coating process.

Since, narrow scan XPS analysis indicated CuO on the surface, we performed XRD analysis to confirm the presence of pure Cu below the coating surface. The obtained XRD pattern is presented in Fig. 9, where the

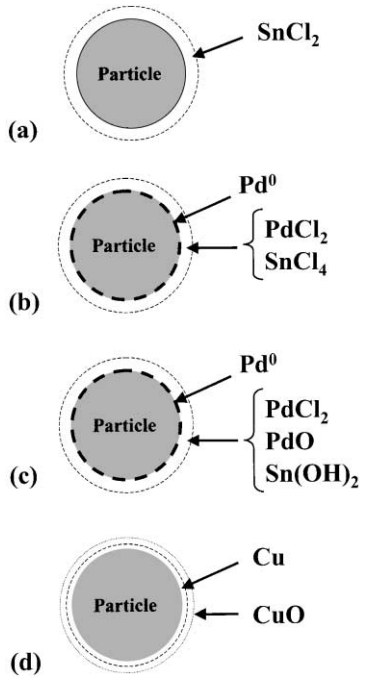

Fig. 10. The proposed mechanism for electroless Cu coating of fly-ash cenosphere particles.

major peaks (1 1 1), (2 0 0) and (2 2 0) of Cu are identified by comparison with the PDF card (no. 04-0836) of JADE-SCAN software, revealing its FCC structure. This confirmed the successful deposition of pure Cu by the present electroless technique. It is to be noted that XPS scans only 3 nm thickness below the surface while XRD spectrum corresponds to approximately 1 μm thickness. Since in the present investigation, the Cu coating thickness varying from 200 nm to 1 μm are obtained, depending upon the coating conditions, the oxidation of Cu as indicated by XPS is a mere surface phenomenon and bulk pure Cu exists below this oxidized layer.

From the overall broad and narrow scan XPS analysis, as discussed above, we now propose the mechanism of electroless Cu coating of fly cenosphere particles investigated here, and is presented schematically in Fig. 10. After the sensitization of the cenosphere particles (Fig. 10(a)), $SnCl_2$ gets deposited on the cenosphere particle surface. Subsequent activation of the sensitized particles results in the deposition of Pd^0 clusters of size 5–6 nm, due to the reduction of

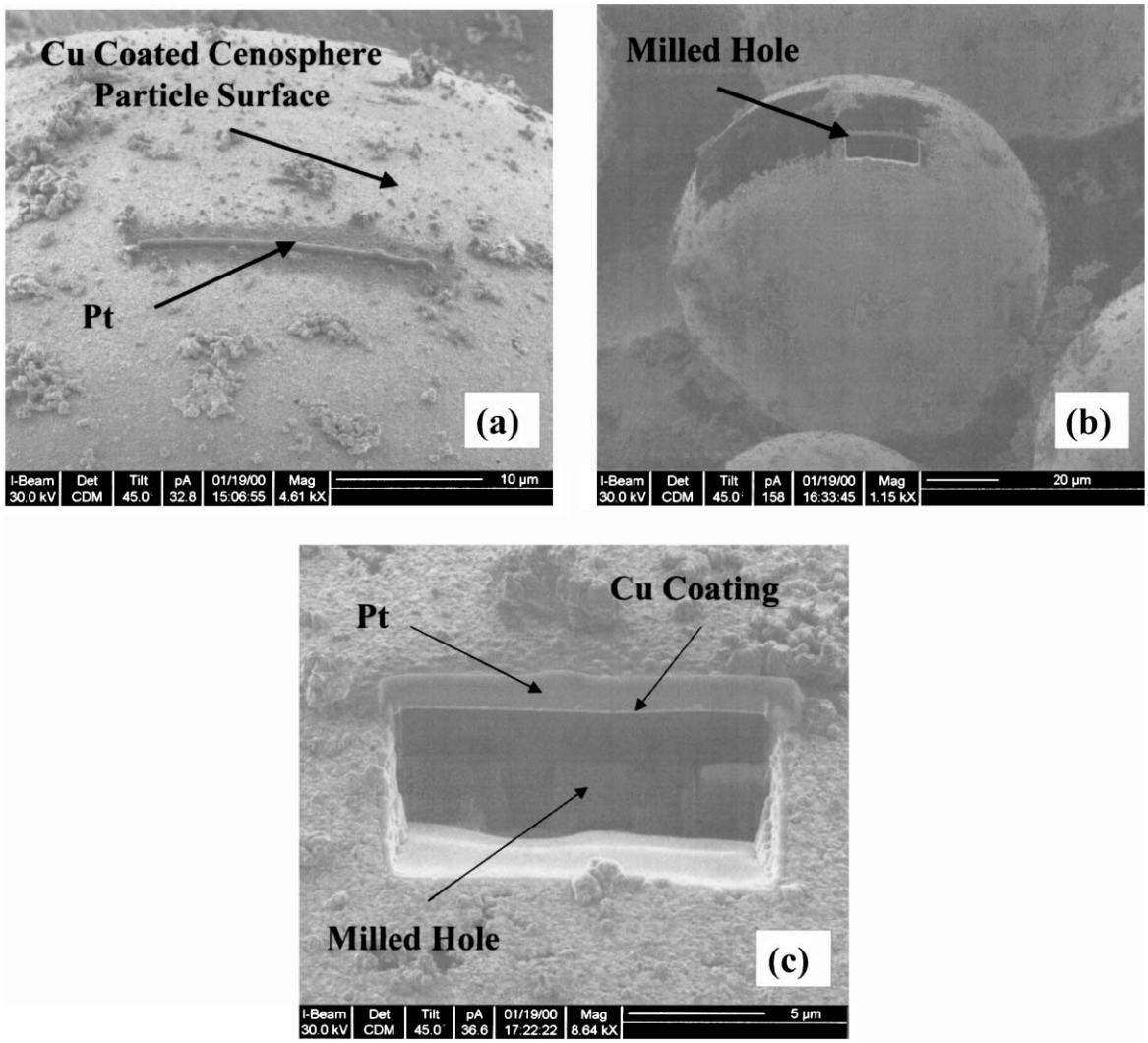

Fig. 11. Steps involved during the Cu coating thickness measurement via FIB technique. (a) Deposition of solid Pt on the surface of Cu-coated fly-ash cenosphere particle; (b) Cu-coated fly-ash cenosphere particle with a milled hole and (c) milled hole at high magnification.

$PdCl_2$ by $SnCl_2$ (Fig. 10(b)). The presence of $PdCl_2$ as residual reactant and $SnCl_4$ as a reaction product might be detected on the particle surface. Even after thorough washing in de-ionized water, these species may not get completely dissolved; instead result in the formation of PdO along with a sheath of $Sn(OH)_2$ and $PdCl_2$ (Fig. 10(c)), which cover the Pd^0 catalytic sites. However, the coating bath first dissolves this sheath, exposing the Pd^0 sites for actual Cu deposition. The Cu coating begins at this point, when Cu atoms formed by the reduction of Cu^{2+} ions by HCHO are deposited on the cenosphere particle surface, the reaction which is activated by Pd^0 sites. Deposited Cu atoms then act as self-catalyst for subsequent Cu deposition and uniform Cu coating develops via formation and growth of Cu nanoparticles. During the

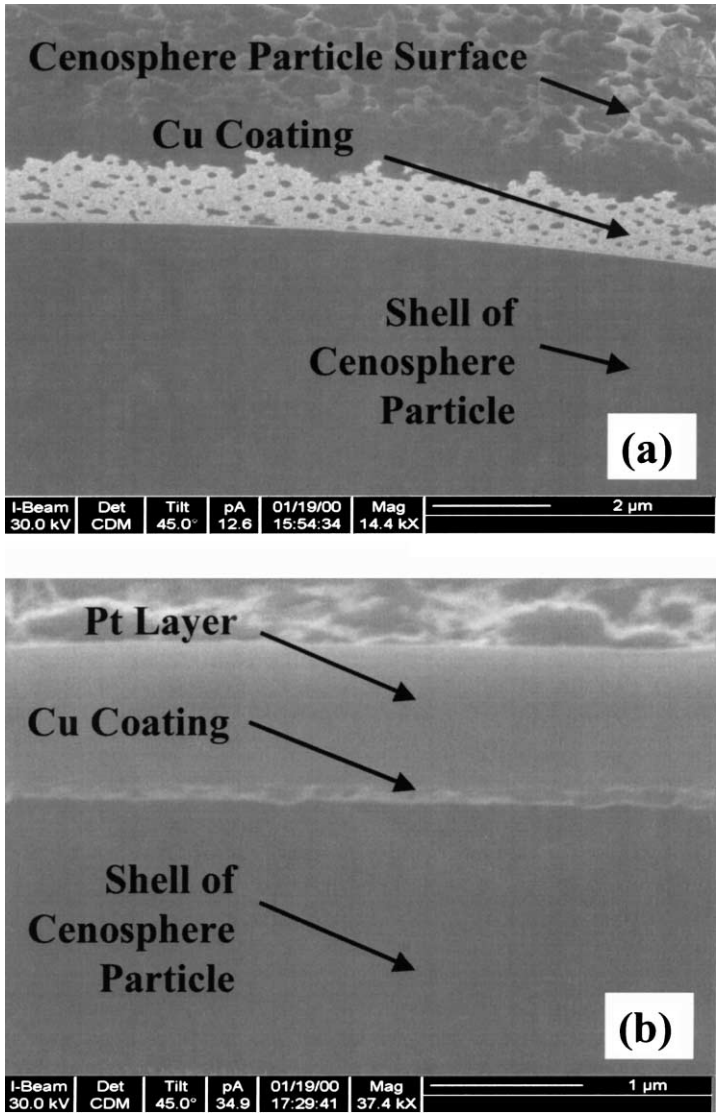

Fig. 12. FIB micrographs showing the Cu coating developed on the fly-ash cenosphere particles (batch-I) surfaces. In (a) 5 g and in (b) 50 g of samples is coated and the respective Cu coating thickness is calculated to be — (a) 1.2 μm and (b) 300 nm.

growth process, Cu may get partially oxidized to CuO at the surface, however, pure metallic Cu remains below this oxidized layer (Fig. 10(d)).

3.3. Thickness measurement via FIB

As mentioned earlier FIB was used to measure directly the Cu coating thickness under various processing conditions. The steps involved in the thickness measurement via FIB have already been described earlier in this article and are also presented in Fig. 11. As exhibited by Fig. 11(a), first a thin strip of Pt is deposited on the Cu-coated cenosphere surface, which is followed by milling a hole near the edge of the Pt deposit (Fig. 11(b)). The milled hole at high magnification is shown in Fig. 11(c), through which a direct measurement of Cu coating thickness is possible at still higher magnifications.

Five and 50 g of cenosphere particles from the batch-I were used for the initial two coating experiments to

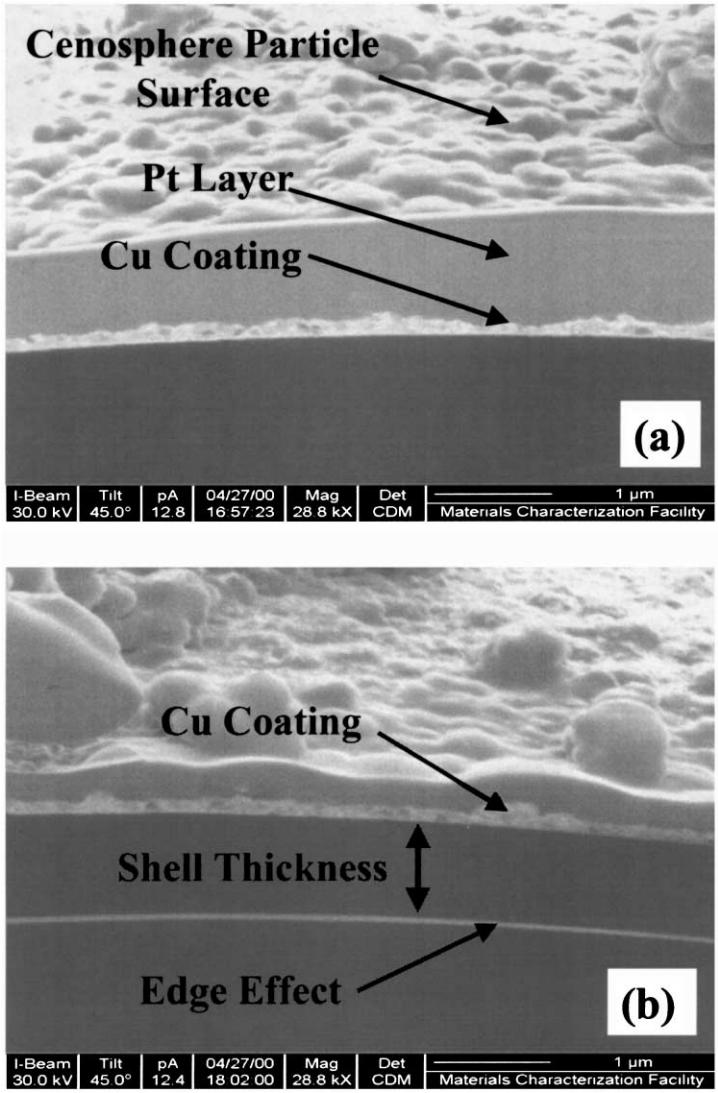

Fig. 13. FIB micrographs showing the Cu coating developed on the fly-ash cenosphere particles (batch-I) with $PdCl_2$ concentration — (a) 1.0 g/l and (b) 0.5 g/l. The respective Cu coating thickness is calculated to be — (a) 250 nm and (b) 200 nm.

study the effect of surface area on the coating thickness, which was measured via FIB technique and the corresponding micrographs are presented in Fig. 12. From Fig. 12(a), the Cu coating thickness of 1.2 μm is calculated and it corresponds to 5 g of sample. Although, the Cu coating is seen to be porous, it is highly continuous and uniform in thickness. The porous nature of coating may be a result of entrapment of hydrogen gas (see reactions (2)–(4)). In Fig. 12(b), which corresponds to 50 g sample, the Cu coating thickness is calculated to be 300 nm. Comparison of the coating thickness in Fig. 12(a) and (b) shows that the total surface area of the particles required to be coated strongly affects the Cu coating thickness. Smaller the initial weight of the sample, minimum is the total surface area required to be coated, and hence, larger is the coating thickness and vice versa.

In another experiment, $PdCl_2$ concentration was varied to understand its effect on the coating thickness and the results are presented in Fig. 13. 5 g of cenosphere particles from batch-II was used for this purpose. The Cu coating thickness of 250 nm was observed when $PdCl_2$ concentration was 1.0 g/l (Fig. 13(a)). The coating thickness was reduced to 200 nm by decreasing the $PdCl_2$ concentration to 0.5 g/l (Fig. 13(b)). The Cu coating in Fig. 13(a) is further observed to be denser than that in Fig. 13(b). The thicker and denser Cu coating in Fig. 13(a) can be directly attributed to large number of catalytic nuclei provided for Cu deposition by large $PdCl_2$ concentration. Interestingly, in Fig. 13(b), the shell thickness of the hollow cenosphere particle is clearly visible and is calculated to be approximately $\sim$1 μm thick. Thus, it is to be noted here that the variation in the coating thickness as a function of coating variables can be studied precisely by the use of FIB, which appears to be the most convenient technique to measure directly the Cu coating thickness.

In summary, the electroless Cu coating of fly-ash cenosphere particles has been successfully demonstrated and characterized completely for better understanding of the coating process.

4. Conclusions

1. Fly-ash cenosphere particles are successfully coated by electroless Cu coating process utilizing Sn–Pd catalyst system. This is the first article in the open literature to report the electroless Cu coating of fly-ash cenosphere particles.
2. The mechanism of electroless Cu coating process of fly-ash cenosphere particles is studied with the help of XPS, which involves sensitization and activation of the fly-ash cenosphere particle surface by $SnCl_2$ and $PdCl_2$, respectively, to deposit pure Pd^0 clusters of size 5–6 nm, which act as a nucleation sites for subsequent Cu-deposition. The sheath of $Sn(OH)_2$ and $PdCl_2$ which covers the Pd^0 sites after the washing step, appears to be dissolved by the coating bath itself exposing the Pd^0 sites for subsequent Cu-deposition. The Cu atoms then act as self-catalyst and the uniform Cu coating then develops via formation and growth of Cu nanoparticles. The CuO formed in this electroless coating process is a mere surface oxide while pure Cu exists below this oxidized layer.
3. The concept of +ve BE shift with the cluster size can be utilized to predict the average Pd^0 cluster size, which acts as a catalyst for Cu-deposition, from the core-level BE shift observed for Pd $3d_{5/2}$ spectrum.
4. Focused ion beam microscopy is a powerful technique to measure directly the Cu coating thickness obtained over the fly-ash cenosphere particle surface. This is the first article to demonstrate the use of FIB for measuring the Cu coating thickness obtained over the fly-ash cenosphere particle surface.

Acknowledgements

Authors take this opportunity to thanks Energy Strategy Associates, Inc. (USA), Coal Resources, Inc. (USA) and I4 Corridor Initiative for financial support. Authors also acknowledge AMPAC's Materials Characterization Facility.

References

[1] M.S. Devi, V. Murugesan, K. Rengaraj, P. Anand, J. Appl. Polym. Sci. 69 (1998) 1385.
[2] M.H. Maher, P.N. Balaguru, J. Mater. Civil Eng. 5 (1993) 212.
[3] C.S. Ramesh, S.K. Seshadari, K.J.L. Iyer, Wear 145 (1991) 189.

[4] D. Deonath, P.K. Rohatgi, J. Mater. Sci. 16 (1981) 1599.
[5] D.S. Yas, V.I. Pavlenko, V.B. Podmokov, Poroshk. Metall. 1 (1976) 31.
[6] D.S. Coleman, J.N. Foba, Powder Metall. 32 (1989) 35.
[7] M. Punovic, M. Schlesinger, Fundamentals of Electrochemical Deposition, Wiley, New York, 1998, p. 133.
[8] T.L. Barr, S. Seal, J. Vac. Sci. Tech. A 13 (1995) 1239.
[9] P.M.A. Sherwood, in: D. Briggs, M.P. Seah (Eds.), Practical Surface Analysis by Auger and Photoelectron Spectroscopy, Wiley, London, 1983, p. 445.
[10] P.M.A. Sherwood, in: D. Briggs, M.P. Seah (Eds.), Data Analysis in XPS and AES in Practical Electron Spectroscopy, Appendix 3, Wiley, New York, 1990, p. 555.
[11] N.M.D. Brown, J.A. Hewitt, B.J. Meenan, Surf. Interface Anal. 20 (1993) 215.
[12] W.E. Modderman, W.C. Bowling, D.C. Carter, D.R. Grove, Surf. Interface Anal. 11 (1988) 317.
[13] B.J. Meenan, N.M.D. Brown, J.W. Wilson, Appl. Surf. Sci. 74 (1994) 221.
[14] M.G. Mason, Phys. Rev. B 27 (1983) 748.
[15] S. Shukla, S. Seal, Nanostructured Mater. 11 (1999) 1181.
[16] Y. Takasu, R. Unwin, B. Tesche, A.M. Bradshaw, Surf. Sci. 77 (1978) 219.
[17] G.K. Wertheim, S.B. DiCenzo, D.N.E. Buchanan, Phys. Rev. B 33 (1986) 5384.
[18] K.S. Kim, N. Winogard, Chem. Phys. Lett. 30 (1975) 91.
[19] K.S. Liang, W.R. Salaneck, I.A. Aksay, Solid State Commun. 19 (1976) 329.
[20] J.F. Moulder, W.F. Stickle, P.E. Sobot, K.D. Bomben, in: J. Chastain (Ed.), Handbook of X-ray Photoelectron Spectroscopy: A Reference Handbook of Standard Spectra for Identification and Interpretation of XPS Data, Perkin-Elmer, Minnesota, 1992, p. 234.